THE JOURNAL OF PHYSICAL CHEMISTRY C

Article

pubs.acs.org/JPCC

Spin−Orbit Gaps in Carbynes

Pavel N. D'yachkov* and Vasiliy A. Zaluev

Kurnakov Institute of General and Inorganic Chemistry of the Russian Academy of Sciences, Leninskii pr. 31, 119991 Moscow, Russia

ABSTRACT: The effect of spin−orbit interaction on the band structures of the monatomic carbon chains, called the carbynes, is calculated in terms of a linear augmented cylindrical wave method. Because of the cylindrical symmetry of carbynes, the twofold orbitally degenerate π bands correspond to the semiclassical clockwise and anticlockwise rotational motion of electrons around the symmetry axis. In the absence of spin−orbit interaction with the two possible directions of spin, the π bands would be the fourfold degenerate ones. The spin and orbital motion of electrons are coupled, thereby splitting the fourfold degeneracy. Each π sub-band still has the twofold degeneracy, the spin polarization direction between degenerate two bands being opposite to each other. In a cumulenic carbyne with the double bonds (...=C=C=...), the splitting of π band at the Fermi energy region is equal to 2.4 meV, but the metallic character of band structure is not broken by spin−orbit interaction. In the semiconducting polyynic carbyne with alternating single and triple bonds (...−C≡C−C≡C−...), the spin−orbit gaps are different for the highest valence band (3.1 meV) and the lowest conduction band (2.1 meV). The spin−orbit gaps in carbyne are about 2 or 3 times smaller than the spin−orbit splitting (6 meV) in the carbon atom. In carbyne, the spin−orbit interaction is larger than that in carbon nanotubes because of the larger curvature of electron orbits encircling the carbyne chains; the larger spin−orbit coupling can be attractive for new experiments and applications.

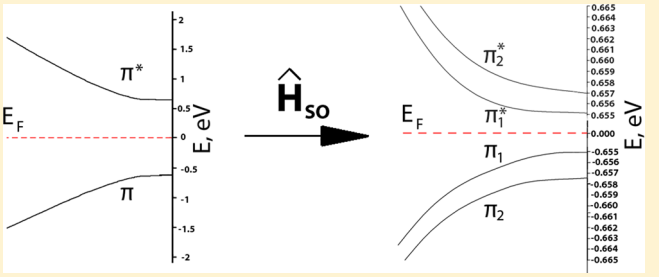

1. INTRODUCTION

In carbon nanomaterials, the interaction of the spin of electrons with their orbital motion has become a focus of great attention in the past decade. Previously, on the basis of low atomic number of carbon, the spin−orbit effects were commonly assumed to be negligible. An example of this is flat graphene in which the spin−orbit splitting effects appear at energy scales of only 10^{-3} meV.[1] The situation changed in 2000 when the first theoretical study of spin−orbit interaction in carbon nanotubes was done.[2] In terms of the *kp*-method, it was shown that the curvature of the nanotube surface breaks a symmetry that is present in graphene; this broken symmetry enhances the intrinsic spin−orbit coupling in carbon nanotubes compared with flat graphene, and the spin−orbit term gives rise to the splitting of energy levels and formation of gaps about 0.1 meV. The curvature-induced spin−orbit splitting in the Fermi level region of nanotubes was also studied in terms of the empirical tight-binding models,[3−7] in addition to the first-principle projected augmented wave[8] and linear augmented cylindrical wave methods.[9] The spin−orbit effects were also qualitatively studied in the curved graphene, fullerene, and nanotube caps in terms of simple π-electron model and perturbation theory, the importance of curvature of a carbon material surface for larger spin−orbital coupling being indicated again.[10] In 2008, the predicted spin−orbital gaps for the nanotubes were detected using the ultra-low-temperature measurements of the intrinsic electronic spectrum of the ultraclean nanotube quantum dot, the spin−orbit splitting Δ_{S-O} being equal to 0.37 and 0.21 meV for the electrons and holes, respectively.[11] The spin−orbit coupling was also revealed by direct current magneto-conductance and spectroscopy for the complementary situations of the open nanotube quantum wire and quantum dot in the multielectron regime and in the presence of finite disorder.[12−14] Now the situation is promising for applications of the spin−orbit interaction effects in carbon nanotubes devices. For example, it is demonstrated that carbon nanotubes are promising candidates for memory devices with fast magnetization switching; they are excellent spin-current waveguides[15,16] and allow spin control[17] and spin filtering.[18] The spin−orbital coupling enables fast electrical spin manipulation in carbon nanotube spin qubits;[17,19] it can influence the Josephson supercurrents in nanotube superconducting junctions,[20] allows the spin to couple with the high-quality vibrational modes of nanotubes,[21,22] and can affect electron spin decoherence in nanotube quantum dots.[23]

The aim of this work is to calculate the effects of spin−orbit interaction on the band structures of the monatomic carbon chains. These chains, called the carbynes, are the most simple carbon molecular systems that may be of interest as the potential materials for nanoelectronics and spintronics. The existence of stable long linear carbon chains is now reliably established (e.g., see references in ref 24). According to a valence of the carbon atoms, formation of the two structural forms with the translational unit cells having one and two carbon atoms is possible for the linear carbon chains. In a cumulenic form of carbyne, the C atoms form the double bonds

Received: October 11, 2013
Revised: December 15, 2013

   dx.doi.org/10.1021/jp410108f | J. Phys. Chem. C XXXX, XXX, XXX−XXX

(...=C=C=...), but the single and triple bonds alternate in the polyynic structure (...−C≡C−C≡C−...). In carbyne, the spin−orbital interaction must be larger than that in carbon nanotubes. The reason is the larger curvature of electron orbits encircling the carbyne chains compared to that of carbon nanotube surface. The larger spin−orbit coupling can be attractive for new experiments and applications.

2. METHOD OF CALCULATION

We calculated the complete band structure of carbynes in terms of a linear augmented cylindrical wave (LACW) method.[25−27] The LACW method is just a reformulation of the linear augmented plane wave method for cylindrical multiatomic systems. We use structural information as input parameters.[25−27] For the achiral carbon nanotubes, the LACW technique with account of the spin−orbit coupling is presented in ref 9; this theory is easily rewritten for the case of carbynes. We use the two-component Hamiltonian written in terms of atomic units of Rydberg:[28,29]

$$H = -\Delta + V + \frac{1}{c^2}\boldsymbol{\sigma}\cdot[(\nabla V) \times \mathbf{p}] \quad (1)$$

The first two terms include the kinetic energy $-\Delta$ and potential energy V and correspond to the nonrelativistic Hamiltonian operator $H_0 = -\Delta + V$. The third term is the operator of the spin−orbit interaction H_{S-O}. Here, c is the speed of light, $\mathbf{p}$ is the momentum operator, and $\boldsymbol{\sigma}$ is the Pauli matrix:

$$\sigma_1 = \begin{pmatrix} 0 & 1 \\ 1 & 0 \end{pmatrix}, \sigma_2 = \begin{pmatrix} 0 & -i \\ i & 0 \end{pmatrix}, \sigma_3 = \begin{pmatrix} 1 & 0 \\ 0 & -1 \end{pmatrix} \quad (2)$$

As the nonrelativistic part of Hamiltonian makes the major contribution to the energy, it is possible to use the following procedure.[30] First, we find the eigenfunctions $\Psi^0_{n,k}(\mathbf{r})$ and eigenvalues $E^0_n(k)$ of the nonrelativistic Hamiltonian, using a previously developed method.[25−27] Then we double the basis to include the spin $\Psi^0_{n,k}(\mathbf{r},\chi) = \Psi^0_{n,k}(\mathbf{r})\chi$; here, $\chi = \alpha$ or β are the pure spin functions. It remains to calculate the matrix elements of the H_{S-O} using the spinor basis $\Psi^0_{n,k}(\mathbf{r})\chi$

$$\langle \Psi^0_{n_2,k}(\mathbf{r})\chi_2 | H | \Psi^0_{n_1,k}(\mathbf{r})\chi_1 \rangle = \varepsilon_{n_1}\delta_{n_2,n_1}\delta_{\chi_2,\chi_1} + \langle \Psi^0_{n_2,k}(\mathbf{r})\chi_2 | H_{S-O} | \Psi^0_{n_1,k}(\mathbf{r})\chi_1 \rangle \quad (3)$$

With due account of the spin−orbit coupling, the energies and wave functions are calculated by diagonalizing this matrix.

2.1. Cylindrical Muffin-Tin Potential. In the LACW method, the approximations are made in the sense of muffin-tin (MT) potentials and local density functional theory only. Starting from an electron density of system as the superposition of the atomic ones, the electronic potential is constructed to be spherically symmetrical in the regions of MT spheres Ω_I and constant in the interspherical region Ω_{II}. Inside the MT spheres, we calculate the electron potential by means of the local-density approximation with Slater exchange. As usual, the radii of the MT spheres ($r_{\alpha_{MT}}$) were chosen so that the atomic spheres touch but do not overlap. The atoms of carbynes are surrounded by essentially impenetrable cylinder-shaped potential barrier because there is a vacuum region on the outside of the wires and an infinite motion of electron is obviously limited in the case of monatomic wires by their size and shape. On the basis of our previous LACW calculations of the carbon systems,[25−27] the radius a = 2.3 au of the barrier is chosen so that the region confined by a barrier accommodates a significant portion of the electron density of the system.

2.2. Basis Functions. Now, let us present the necessary information about the way of calculating of the eigenfunctions $\Psi^0_{n,k}(\mathbf{r})$ of the nonrelativistic LACW method.[25−27] Initially, we define the basic functions that are the solutions of the Schrödinger equation for interspherical and MT regions. In the interspherical region, the basis functions $\Psi^k_{PMN}(\mathbf{r})$ are the solutions of the Schrödinger equation for a free electron motion in the cylindrical potential well, which in terms of the cylindrical coordinates (Z, Φ, R) is written as

$$\left\{-\left[\frac{1}{R}\frac{\partial}{\partial R}\left(R\frac{\partial}{\partial R}\right) + \frac{1}{R^2}\frac{\partial^2}{\partial \Phi^2} + \frac{\partial^2}{\partial Z^2}\right] + V(R)\right\} \times \Psi(Z, \Phi, R) = E\Psi(Z, \Phi, R) \quad (4)$$

with $V(R) = 0$ for $R \le a$ and $V(R) = \infty$ for $R > a$. The solutions, called the cylindrical waves, are presented in the textbooks on quantum mechanics.[31,32] Because of the cylindrical symmetry of the potential $V(R)$, the cylindrical waves are written as $\Psi(Z, \Phi, R) = \Psi^k_P \Psi_M(\Phi)\Psi_{MN}(R)$. Here, the Bloch function $\Psi^k_P(Z)$ describes the free electron movement along the Z-axis in the system with translational period d

$$\Psi^k_P(Z) = (1/\sqrt{d})\exp[i(k + k_P)Z]; \quad 0 \le k \le \pi/d; \quad k_P = (2\pi/d)P \text{ with } P = 0, \pm1, \pm2, \ldots \quad (5)$$

The functions $\Psi_M(\Phi) = e^{iM\Phi}/(2\pi)^{1/2}$, where $M = 0, \pm1, \pm2, \ldots$, correspond to the rotation of an electron about the Z-axis. The functions $\Psi_{MN}(R)$ describe the radial movement of an electron in the interspherical regions. They are the solutions of the equation:

$$\left[-\frac{1}{R}\frac{\mathrm{d}}{\mathrm{d}R}R\frac{\mathrm{d}}{\mathrm{d}R} + \frac{M^2}{R^2} + V(R)\right]\Psi_{MN}(R) = E_{|M|,N}\Psi_{MN}(R) \quad (6)$$

The cylindrical waves energy $E = (k + k_P)^2 + E_{|M|,N}$. For $R \le a$, the eq 6 takes the form of the Bessel equation[3234]

$$\left[\frac{\mathrm{d}^2}{\mathrm{d}R^2} + \frac{1}{R}\frac{\mathrm{d}}{\mathrm{d}R} + \kappa_{|M|,N}{}^2 - \frac{M^2}{R^2}\right]\Psi_{MN}(R) = 0 \quad (7)$$

with $\kappa_{|M|,N} = \{E_{|M|,N}\}^{1/2}$. The solutions of eq 7 are the cylindrical Bessel functions of the first J_M kind $\Psi_{MN}(R) = C_{M,N}J_M(\kappa_{|M|,N}R)$. The condition of the vanishing of $\Psi_{MN}(R)$ at the impenetrable barrier $\Psi_{MN}(a) = J_M(\kappa_{|M|,N}a) = 0$ determines the energy spectrum $E_{|M|,N} = (\alpha_{|M|,N})^2/a^2$. Here, $\alpha_{|M|,N}$ is the Nth root of the Bessel function of the Mth order (N = 1, 2, ...). The constant $C_{MN} = (2)^{1/2}/\{a|J'_M|(\kappa_{|M|,N}\alpha)\}$, where J'_M is the derivative of the Bessel function, is determined from the normalization of the $\Psi_{MN}(R)$. Finally, in the cylindrical coordinate system (Z, R, Φ) and in the local spherical coordinate system (ρ, θ, φ) centered on the atom α_{MT} ($Z_{\alpha_{MT}}$, 0, 0), the cylindrical wave takes the form

$$\Psi^{PMN,k}_{II}(Z, \Phi, R) = \{\sqrt{\Omega}|J'_M(\kappa_{|M|,N}a)|\}^{-1} \times \exp\{i[(k + k_P)Z + M\Phi]\}J_M(\kappa_{|M|,N}R) \quad (8)$$

dx.doi.org/10.1021/jp410108f | J. Phys. Chem. C XXXX, XXX, XXX−XXX

$$\Psi^{PMN,k}_{\mathrm{II},\alpha_{\mathrm{MT}}}(\rho,\theta,\varphi) = \{\sqrt{\Omega}|J'_M(\kappa_{|M|,N}a)|\}^{-1}\exp\{i[(k+k_P)Z_{\alpha_{\mathrm{MT}}}]\}$$
$$\exp\{i[(k+k_P)\rho\cos\theta]\}J_M(\kappa_{|M|,N}\rho\sin\theta)e^{iM\varphi} \quad (9)$$

where $\Omega = \pi a^2 d$.

Inside the MT sphere α_{MT} in the local spherical coordinate system, the basis function is expanded in spherical harmonics $Y_{lm}(\theta,\varphi)$

$$\Psi^{PMN,k}_{\alpha_{\mathrm{MT}}}(\rho,\theta,\varphi) = \sum_{l=0}^{\infty}\sum_{m=-l}^{l}[A^{PMN,k}_{lm,\alpha_{\mathrm{MT}}}u_{l,\alpha_{\mathrm{MT}}}(\rho,E_{l,\alpha_{\mathrm{MT}}}) + B^{PMN,k}_{lm,\alpha_{\mathrm{MT}}}\dot{u}_{l,\alpha_{\mathrm{MT}}}(\rho,E_{l,\alpha_{\mathrm{MT}}})]Y_{lm}(\theta,\varphi) \quad (10)$$

Here, $u_{l,\alpha_{\mathrm{MT}}}$ are the solutions of the radial Schrödinger equation for the local density spherically symmetric potential $V_{\alpha_{\mathrm{MT}}}$ and energy $E_{l,\alpha_{\mathrm{MT}}}$

$$\frac{1}{\rho}\frac{\mathrm{d}^2\rho u_{l,\alpha_{\mathrm{MT}}}(\rho)}{\mathrm{d}\rho^2} + \left(E_{l,\alpha_{\mathrm{MT}}}V_{\alpha_{\mathrm{MT}}}(\rho) - \frac{l(l+1)}{\rho^2}\right)u_{l,\alpha_{\mathrm{MT}}}(\rho) = 0 \quad (11)$$

and $\dot{u}_{l,\alpha_{\mathrm{MT}}} = [\partial u_{l,\alpha_{\mathrm{MT}}}/\partial E]_{E_{l,\alpha\mathrm{MT}}}$. Equating the values of the function $\Psi^{PMN,k}_{\mathrm{II},\alpha_{\mathrm{MT}}}(\rho,\theta,\varphi)|_{\rho=r_{\alpha\mathrm{MT}}}$ (9) and $\Psi^{PMN,k}_{\alpha_{\mathrm{MT}}}(\rho,\theta,\varphi)|_{\rho=r_{\alpha\mathrm{MT}}}$ (10) as well as their values of derivatives with respect to the radius $\partial[\Psi^{PMN,k}_{\mathrm{II},\alpha_{\mathrm{MT}}}(\rho,\theta,\varphi)]/\partial\rho|_{\rho=r_{\alpha\mathrm{MT}}}$, $\partial[\Psi^{PMN,k}_{\alpha_{\mathrm{MT}}}(\rho,\theta,\varphi)]/\partial\rho|_{\rho=r_{\alpha\mathrm{MT}}}$, the constants $A^{PMN,k}_{lm,\alpha_{\mathrm{MT}}}$ and $B^{PMN,k}_{lm,\alpha_{\mathrm{MT}}}$ can be chosen so that the basis functions $\Psi^{k}_{PMN}(\mathbf{r})$, called the linear augmented cylindrical waves, and their first derivatives are continuous everywhere including the boundaries of the MT spheres. For monatomic wires, the nonzero values of $A^{PMN,k}_{lm,\alpha_{\mathrm{MT}}}$ and $B^{PMN,k}_{lm,\alpha_{\mathrm{MT}}}$ correspond to $m = M$

$$A^{PMN,k}_{lM,\alpha_{\mathrm{MT}}} = {r_{\alpha_{\mathrm{MT}}}}^2 D^{PMN,k}_{lM,\alpha_{\mathrm{MT}}}a^{PMN,k}_{lM,\alpha_{\mathrm{MT}}},$$
$$B^{PMN,k}_{lM,\alpha_{\mathrm{MT}}} = {r_{\alpha_{\mathrm{MT}}}}^2 D^{PMN,k}_{lM,\alpha_{\mathrm{MT}}}b^{PMN,k}_{lM,\alpha_{\mathrm{MT}}} \quad (12)$$

$$D^{PMN,k}_{lM,\alpha_{\mathrm{MT}}} = \sqrt{\pi}\{\sqrt{\Omega}|J'_M(\kappa_{|M|,N}a)|\}^{-1}(-1)^{(3M+|M|)/2+l}i^l \times\left[\frac{(2l+1)(l-|M|)!}{(l+|M|)!}\right]^{1/2}\exp\{i(k+k_P)Z_{\alpha_{\mathrm{MT}}}\} \quad (13)$$

$$a^{PMN,k}_{lM,\alpha_{\mathrm{MT}}}(r_{\alpha_{\mathrm{MT}}}) = I^{PMN,k}_{2,lM,\alpha_{\mathrm{MT}}}\dot{u}_{l,\alpha_{\mathrm{MT}}}(r_{\alpha_{\mathrm{MT}}}) - I^{PMN,k}_{1,lM,\alpha_{\mathrm{MT}}}\dot{u}'_{l,\alpha_{\mathrm{MT}}}(r_{\alpha_{\mathrm{MT}}}) \quad (14)$$

$$b^{PMN,k}_{lM,\alpha_{\mathrm{MT}}}(r_{\alpha_{\mathrm{MT}}}) = I^{PMN,k}_{1,lM,\alpha_{\mathrm{MT}}}u'_{l,\alpha_{\mathrm{MT}}}(r_{\alpha_{\mathrm{MT}}}) - I^{PMN,k}_{2,lM,\alpha_{\mathrm{MT}}}u_{l,\alpha_{\mathrm{MT}}}(r_{\alpha_{\mathrm{MT}}}) \quad (15)$$

Here, the prime denotes the radial derivative of functions $u_{l,\alpha_{\mathrm{MT}}}$ and $\dot{u}_{l,\alpha_{\mathrm{MT}}}$; finally, I_1 and I_2 are integrals of the augmented Legendre polynomials $P_l^{|M|}$

$$I^{PMN,k}_{1,lM,\alpha_{\mathrm{MT}}} = 2\int_0^{\pi/2}\exp\{ik_P r_{\alpha_{\mathrm{MT}}}\cos\theta\}J_M(\kappa_{|M|,N}r_{\alpha_{\mathrm{MT}}}\sin\theta) \times P_l^{|M|}(\cos\theta)\sin\theta\,\mathrm{d}\theta \quad (16)$$

$$I^{PMN,k}_{2,lM,\alpha_{\mathrm{MT}}} = 2\int_0^{\pi/2}\exp\{i(k_P r_{\alpha_{\mathrm{MT}}}\cos\theta)\}\{ik_P \times\cos\theta\,J_M(k_{|M|,N}r_{\alpha_{\mathrm{MT}}}\sin\theta) + (1/2)k_{|M|,N}\sin\theta\} \times[J_{M-1}(k_{|M|,N}r_{\alpha_{\mathrm{MT}}}\sin\theta) - J_{M+1}(k_{|M|,N}r_{\alpha_{\mathrm{MT}}} \times\sin\theta)]\}P_l^{|M|}(\cos\theta)\sin\theta\,\mathrm{d}\theta \quad (17)$$

The methods of solving the nonrelativistic Schrödinger equation using the basis of the linear augmented cylindrical waves $\Psi^{k}_{PMN}(\mathbf{r})$ is described in the works (25)−(27). The results of this calculation are the nonrelativistic energy $E^0_n(k)$ of different bands n at different points k of the Brillouin zone and the spin-independent wave functions $\Psi^0_{n,k}(\mathbf{r})$ represented as the linear combinations of basis functions

$$\Psi^0_{n,k}(\mathbf{r}) = \sum_{PMN}a^{kn}_{PMN}\Psi^{k}_{PMN}(\mathbf{r}) \quad (18)$$

2.3. Matrix Elements of the Spin−Orbit Interaction.

Now, we can use the spin-dependent basis $\Psi^{k}_{PMN}(\mathbf{r},\alpha) = \Psi^{k}_{PMN}(\mathbf{r})\alpha$, $\Psi^{k}_{PMN}(\mathbf{r},\beta) = \Psi^{k}_{PMN}(\mathbf{r})\beta$ for calculating the matrix elements of the spin−orbit interaction. For the spherically symmetric potential of each MT sphere $V_{\alpha_{\mathrm{MT}}}(\rho)$, this operator can be written using the angular momentum operator as follows:[30]

$$H_{\mathrm{S-O}} = \frac{1}{c^2}\boldsymbol{\sigma}\cdot[(\nabla V_{\alpha_{\mathrm{MT}}})\times\mathbf{p}] = \frac{1}{c^2}\frac{1}{\rho}\frac{\mathrm{d}V_{\alpha_{\mathrm{MT}}}}{\mathrm{d}\rho}\boldsymbol{\sigma}\mathbf{L} = \frac{1}{c^2}\frac{1}{\rho}\frac{\mathrm{d}V_{\alpha_{\mathrm{MT}}}}{\mathrm{d}\rho}\left(\frac{1}{2}\sigma_+L_- + \frac{1}{2}\sigma_-L_+ + \sigma_zL_z\right) \quad (19)$$

The action of the spin operator on the function of α and β is described by the equations

$$\sigma_+\alpha = 0,\ \sigma_-\alpha = 2\beta,\ \sigma_z\alpha = \alpha,\ \sigma_+\beta = 2\alpha,\ \sigma_-\beta = 0,\ \sigma_z\beta = -\beta \quad (20)$$

The action of the angular momentum operator on spherical harmonics does not affect the radial part of the wave function

$$L_zY_{lm}(\theta\varphi) = mY_{lm}(\theta\varphi),\quad L_\pm Y_{lm}(\theta\varphi) = [l(l+1) - m(m\pm1)]^{1/2}Y_{lm\pm1}(\theta\varphi) \quad (21)$$

As a result, the integrals $\langle\Psi^{k}_{P_2M_2N_2}(\mathbf{r},\chi_2)|H_{\mathrm{S-O}}|\Psi^{k}_{P_1M_1N_1}(\mathbf{r},\chi_1)\rangle$ are represented as the products of integrals over the radial and angular variables. Use of the relations (18)−(20) together with the orthogonality and normalization of the spin functions α and β and of the spherical harmonics allow the angular integration to be performed analytically to give finally

dx.doi.org/10.1021/jp410108f | J. Phys. Chem. C XXXX, XXX, XXX−XXX

$$\langle \Psi^{k}_{P_2,M_2,N_2}(r,\alpha)|H_{S-O}|\Psi^{k}_{P_1,M_1,N_1}(r,\alpha)\rangle = \delta_{M_2,M_1}\frac{\pi}{c^2\Omega}\{J'_{M_1}(\kappa_{|M_1|,N_2}a)J'_{M_1}(\kappa_{|M_1|,N_1}a)\}^{-1}\sum_{\alpha_{MT}} r_{\alpha_{MT}}{}^4 \times \sum_{l=|M_1|}^{\infty}(2l+1)M_1\frac{(l-|M_1|)!}{(l+|M_1|)!}\exp\{i(k_{p_2}-k_{p_1})Z_{\alpha_{MT}}\} \times \{\varsigma_{l,\alpha_{MT}}(a^{P_2,M_1,N_2}_{l,M_1,\alpha_{MT}})^*(a^{P_1,M_1,N_1}_{l,M_1,\alpha_{MT}}) + \ddot{\varsigma}_{l,\alpha_{MT}}(b^{P_2,M_1,N_2}_{l,M_1,\alpha_{MT}}) \times {}^*(b^{P_1,M_1,N_1}_{l,M_1,\alpha_{MT}}) + \dot{\varsigma}_{l,\alpha_{MT}}[(a^{P_2,M_1,N_2}_{l,M_1,\alpha_{MT}})^*(b^{P_1,M_1,N_1}_{l,M_1,\alpha_{MT}}) + (b^{P_2,M_1,N_2}_{l,M_1,\alpha_{MT}})^*(a^{P_1,M_1,N_1}_{l,M_1,\alpha_{MT}})]\} \quad (22)$$

$$\langle \Psi^{k}_{P_2M_2N_2}(\mathbf{r},\beta)|H_{S-O}|\Psi^{k}_{P_1M_1N_1}(\mathbf{r},\beta)\rangle = -\langle \Psi^{k}_{P_2M_2N_2}(\mathbf{r},\alpha)|H_{S-O}|\Psi^{k}_{P_1M_1N_1}(\mathbf{r},\alpha)\rangle \quad (23)$$

$$\langle \Psi^{k}_{P_2,M_2,N_2}(r,\beta)|H_{S-O}|\Psi^{k}_{P_1,M_1,N_1}(r,\alpha)\rangle = \delta_{M_2-1,M_1}\,\mathrm{sign}(M_1) \times \frac{\pi}{c^2\Omega}\{J'_{M_1+1}(\kappa_{|M_1+1|,N_2}a)J'_{M_1}(\kappa_{|M_1|,N_1}a)\}^{-1} \times \sum_{\alpha_{MT}} r_{\alpha_{MT}}{}^4 \sum_{l=|M_1|}^{\infty}[l(l+1)-M_1(M_1+1)]^{1/2} \times \left[\frac{(l-|M_1|)!(l-|M_1+1|)!}{(l+|M_1|)!(l+|M_1+1|)!}\right]^{1/2} \times \exp\{i(k_{p_2}-k_{p_1})Z_{\alpha_{MT}}\}\{\varsigma_{l,\alpha_{MT}}(a^{P_2,M_2,N_2}_{l,M_1+1,\alpha_{MT}}) \times {}^*(a^{P_1,M_1,N_1}_{l,M_1,\alpha_{MT}}) + \ddot{\varsigma}_{l,\alpha_{MT}}(b^{P_2,M_1+1,N_2}_{l,M_1+1,\alpha_{MT}})^*(b^{P_1,M_1,N_1}_{l,M_1,\alpha_{MT}}) + \dot{\varsigma}_{l,\alpha_{MT}}[(a^{P_2,M_2,N_2}_{l,M_1+1,\alpha_{MT}})^*(b^{P_1,M_1,N_1}_{l,M_1,\alpha_{MT}}) + (b^{P_2,M_2,N_2}_{l,M_1+1,\alpha_{MT}}) {}^*(a^{P_1,M_1,N_1}_{l,M_1,\alpha_{MT}})]\} \quad (24)$$

$$\langle \Psi^{k}_{P_2M_2N_2}(\mathbf{r},\alpha)|H_{S-O}|\Psi^{k}_{P_1M_1N_1}(\mathbf{r},\beta)\rangle = \langle \Psi^{k}_{P_2M_2N_2}(\mathbf{r},\beta)|H_{S-O}|\Psi^{k}_{P_1M_1N_1}(\mathbf{r},\alpha)\rangle^* \quad (25)$$

where $\mathrm{sign}(M_1) = 1$ for $M_1 \geq 0$ and $\mathrm{sign}(M_1) = -1$ for $M_1 < 0$; moreover,

$$\varsigma_{l,\alpha_{MT}} = \int_0^{r_{\alpha_{MT}}}[u_{l,\alpha_{MT}}(\rho)]^2\frac{\mathrm{d}V_{\alpha_{MT}}(\rho)}{\mathrm{d}\rho}\rho\,\mathrm{d}\rho \quad (26)$$

$$\dot{\varsigma}_{l,\alpha_{MT}} = \int_0^{r_{\alpha_{MT}}}u_{l,\alpha_{MT}}(\rho)\,\dot{u}_{l,\alpha_{MT}}(\rho)\frac{\mathrm{d}V_{\alpha_{MT}}(\rho)}{\mathrm{d}\rho}\rho\,\mathrm{d}\rho \quad (27)$$

$$\ddot{\varsigma}_{l,\alpha_{MT}} = \int_0^{r_{\alpha_{MT}}}[\dot{u}_{l,\alpha_{MT}}(\rho)]^2\frac{\mathrm{d}V_{\alpha_{MT}}(\rho)}{\mathrm{d}\rho}\rho\,\mathrm{d}\rho \quad (28)$$

The sums over atoms α_{MT} of the unit cell includes one and two atoms for cumulenic and polyynic carbynes, respectively.

3. RESULTS

Figure 1 shows the energy bands of cumulenic and polyynic carbynes. Because of the inversion symmetry, the energy bands at $-k$ are the same as thoat k and they are not shown here. Because of the cylindrical symmetry of carbynes, there are σ- and π-type dispersion curves in the band structures of polyynic and cumulenic systems. The twofold orbitally degenerate π bands correspond to the semiclassical clockwise and anticlockwise rotational motion of electrons around the symmetry axis. In the absence of spin−orbit interaction with the two possible directions of spin, the π bands would be the fourfold degenerate ones. The calculations demonstrate that the spin and orbital motion of electrons are coupled in carbynes, thereby splitting the fourfold degeneracy clearly seen in the insets of the figure. However, each energy π sub-band still has the twofold degeneracy; Kramers theorem on time-reversal symmetry alongside the inversion symmetry of carbynes preserve the spin degeneracy, the spin polarization direction between degenerate two bands being opposite to each other. Obviously, there is no spin−orbit splitting of the orbitally nondegenerate σ bands.

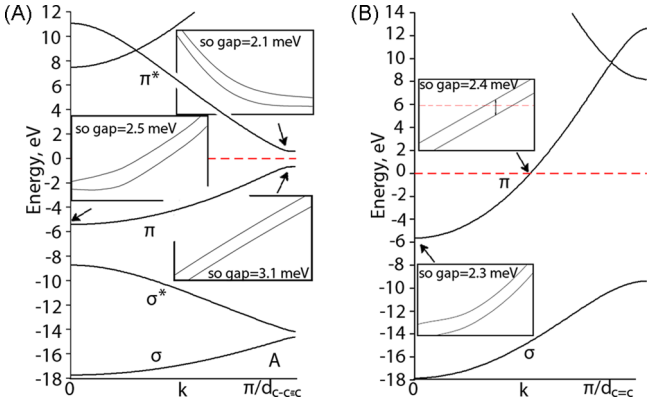

Figure 1. Band structure of polyynic (A) and cumulenic (B) carbynes calculated with account of spin−orbit interaction using LACW method. The calculations were performed for the experimental bond lengths d_{C-C} = 1.360 Å and $d_{C\equiv C}$ = 1.205 Å in polyynic form[35,36] and for the cumulenic bond length $d_{C=C}$ = 1.26 Å.[37]

The polyynic carbyne has the semiconducting-type band structure with a gap between bonding (π) and antibonding (π^*) states equal to 1.14 eV (Figure 1A). The spin−orbit interaction results in the spin−orbit splitting of these valence and conduction bands. Particularly, at the Brillouin zone boundary, the energy splitting induced by the spin−orbit interaction term is different for the highest valence band (3.1 meV) and the lowest conduction band (2.1 meV). For the absence of spin−orbit interaction, metallic cumulenic carbyne would have one π band crossing the Fermi level at the center of the Brillouin zone (Figure 1B). Taking into account the spin−orbit coupling, the band structure becomes more complex and the Fermi energy crosses the two bands. The present calculation shows a direct optical gap equal to 2.5 meV at the Fermi energy region near the point $k = (1/2)(\pi/d_{C-C})$, but the metallic nature for the cumulenic system is not broken by the spin−orbit interaction. The spin−orbit gaps in carbynes are about 2 or 3 times smaller than the spin−orbit splitting (6 meV) in the carbon atom.

4. CONCLUDING REMARKS

We investigated theoretically the band structures of both the cumulenic and polyynic carbynes taking into account the spin−orbit coupling effects. The obtained spin−orbit gaps equal to 2−3 meV are in reasonable agreement with semiclassical model and inverse diameter dependence of the spin−orbit splitting in carbon nanotubes. For example, in the case of the small-diameter (4, 4) nanotube with radius equal to 2.7 Å, the spin−orbit gap calculated using the LACW method is equal to 0.54 meV[9]. For carbyne, a radius of electron orbit is approximately

dx.doi.org/10.1021/jp410108f | J. Phys. Chem. C XXXX, XXX, XXX−XXX

3.5 times smaller; it is about the carbon atomic radius r_C = 0.77 Å. Therefore, the spin−orbit gaps in carbynes are expected to be about 2 meV, in agreement with the LACW calculations. Compare this semiclassical treatment with the Niels Bohr model of atom (1913). Bohr depicts the atom as small, positively charged nucleus surrounded by electrons that travel in circular orbits around the nucleus. Different from the nanotubes, there is no spherical surface in the atom or cylindrical surface in carbynes, but electrons travel in circular orbits; the Bohr model with electrons traveling in circular orbits does not contradict quantum mechanics.

AUTHOR INFORMATION

Corresponding Author

*E-mail: p_dyachkov@rambler.ru. Phone: +79032011976. Fax: +74959541279.

Notes

The authors declare no competing financial interest.

ACKNOWLEDGMENTS

The research was partially supported by the Russian Basic Research Foundation (Grant 14-03-00493) and EU under Project No. FP7-247007 CACOMEL.

REFERENCES

(1) Min, H.; Hill, J. E.; Sinitsyn, N. A.; Sahu, B. R.; Kleinman, L.; MacDonald, A. H. Intrinsic and Rashba Spin-Orbit Interactions in Graphene Sheets. *Phys. Rev. B* **2006**, *74*, 165310.

(2) Ando, T. Spin-Orbit Interaction in Carbon Nanotubes. *J. Phys. Soc. Jpn.* **2000**, *69*, 1757−1763.

(3) Chiko, L.; López-Sancho, M. P.; Miñoz, M. C. Spin Splitting Induced by Spin-Orbit Interaction in Chiral Nanotubes. *Phys. Rev. Lett.* **2004**, *93*, 176402.

(4) Chiko, L.; López-Sancho, M. P.; Miñoz, M. C. Curvature-Induced Anisotropic Spin-Orbit Splitting in Carbon Nanotubes. *Phys. Rev. B* **2009**, *79*, 235423.

(5) Izumida, W.; Sato, K.; Saito, R. Spin−Orbit Interaction in Single Wall Carbon Nanotubes: Symmetry Adapted Tight-Binding Calculation and Effective Model Analysis. *J. Phys. Soc. Jpn.* **2009**, *78*, 074707.

(6) Wunsch, B. Few-Electron Physics in a Nanotube Quantum Dot with Spin-Orbit Coupling. *Phys. Rev. B* **2009**, *79*, 235408.

(7) Liu, H. Band Structures of Carbon Nanotube with Spin−Orbit Coupling Interaction. *Physica B* **2011**, *406*, 104−107.

(8) Zhou, J.; Liang, Q.; Dong, J. Asymmetric Spin-Orbit Coupling in Single-Walled Carbon Nanotubes. *Phys. Rev. B* **2009**, *79*, 195427.

(9) D'yachkov, P. N.; Kutlubaev, D. Spin-Orbit Gaps in Armchair Nanotubes Calculated using the Linear Augmented Cylindrical Wave Method. *IOP Conf. Series: Mater. Sci. Eng.* **2012**, *38*, 012003.

(10) Huertas-Hernando, D.; Guinea, F.; Brataas, A. Spin-Orbit Coupling in Curved Graphene, Fullerenes, Nanotubes, and Nanotube Caps. *Phys. Rev. B* **2006**, *74*, 155426.

(11) Kuemmeth, F.; Ilani, S.; Ralph, D.; McEuen, P. Coupling of Spin and Orbital Motion of Electrons in Carbon Nanotubes. *Nature* **2008**, *452*, 448−452.

(12) Jhang, S. H.; Marganska, M.; Skuorsky, Y.; Preusche, D.; Witkamp, B.; Grifony, M.; van der Zant, H.; Wosnitza, J.; Strank, C. *Phys. Rev. B* **2010**, *82*, 041404.

(13) Jespersen, T.; Grove-Rusmussen, K.; Paaske, J.; Muraki, K.; Fujisawa, T.; Nigård, J.; Flensberg, K. Gate-Dependent Spin-Orbit Coupling in Multielectron Carbon Nanotubes. *Nat. Phys.* **2011**, *7*, 348−353.

(14) Steele, G. A.; Pei, F.; Laird, E. A.; Jol, J. M.; Meerwaldt, H. B.; Kouwenhoven, L. P. Large Spin-Orbit Coupling in Carbon Nanotubes. *Nat. Commun.* **2013**, *4*, 1573.

(15) Guimarães, F. S. M.; Kirwan, D. F.; Costa, A. T.; Muniz, R. B.; Mills, D. L.; Ferreira, M. S. Carbon Nanotube: A Low-Loss Spin-Current Waveguide. *Phys. Rev. B* **2010**, *81*, 153408.

(16) Wang, K. Y.; Blackburn, A. M.; Wang, H. F.; Wunderlich, J.; Williams, D. A. Spin and Orbital Splitting in Ferromagnetic Contacted Single Wall Carbon Nanotube Devices. *Appl. Phys. Lett.* **2013**, *102*, 093508.

(17) Flensberg, K.; Marcus, C. Bends in Nanotubes Allow Electric Spin Control and Coupling. *Phys. Rev. B* **2010**, *81*, 195418.

(18) Gunlycke, D.; Jefferson, J. H.; Bailey, S. W. D.; Lambert, C. J.; Pettifor, D. G.; Briggs, G. A. D. Zener Quantum Dot Spin Filter in a Carbon Nanotube. *J. Phys.: Condens. Matter* **2006**, *18*, S843−S849.

(19) Bulaev, D.; Trauzettel, B.; Loss, D. Spin-Orbit Interaction and AnomalousSpin Relaxation in Carbon Nanotube Quantum Dots. *Phys. Rev. B* **2008**, *77*, 235301.

(20) Lim, J.; López, R.; Aguado, R. Josephson Current in Carbon Nanotubes with Spin-Orbit Interaction. *Phys. Rev. Lett.* **2011**, *107*, 196801.

(21) Pályi, A.; Struck, P.; Rudner, M.; Flensberg, K.; Burkard, G. Spin-Orbit Induced Strong Coupling of a Single Spin to a Nanomechanical Resonator. *Phys. Rev. Lett.* **2012**, *108*, 206811.

(22) Ohm, C.; Stampfer, C.; Splettstoesser, J.; Wegewijs, M. Readout of Carbon Nanotube Vibrations Based on Spin-Phonon Coupling. *Appl. Phys. Lett.* **2012**, *100*, 143103.

(23) Kuemmeth, F.; Churchill, H.; Herring, P.; Marcus, C. Carbon Nanotubes for Coherent Spintronics. *Mater. Today* **2010**, *13*, 18−26.

(24) D'yachkov, P. N.; Zaluev, V. A.; Kocherga, E. Yu.; Sadykov, N. R. Tight Binding Model of Quantum Conductance of Cumulenic and Polyynic Carbynes. *J. Phys. Chem. C* **2013**, *117*, 16306−16315.

(25) D'yachkov, P. N. Augmented Waves for Nanomaterials. In *Encyclopedia of Nanoscience and Nanotechnology*; Nalwa, H. S., Ed.; American Scientific: Valencia, CA, 2004; Vol. *1*, pp 191−212.

(26) D'yachkov, P. N.; Makaev, D. V. Account of Helical and Rotational Symmetries in the Linear Augmented Cylindrical Wave Method for Calculating the Electronic Structure of Nanotubes: Towards the *ab initio* Determination of the Band Structure of a (100, 99) Tubule. *Phys. Rev. B* **2007**, *76*, 195411.

(27) D'yachkov, P. N.; Kutlubaev, D. Z.; Makaev, D. V. Linear Augmented Cylindrical Wave Green's Function Method for Electronic Structure of Nanotubes with Substitutional Impurities. *Phys. Rev. B* **2010**, *82*, 035426.

(28) Davydov, A. S. *Quantum mechanics*, 2nd ed.; Pergamon Press: Oxford; New York, 1965.

(29) Schiff, L. I. *Quantum Mechanics*; McGraw-Hill: New York, 1949; 404 pp.

(30) Conklin, J B; Johnson, L E; Pratt, G W *Phys. Rev.* **1965**, *137 4A*, 1283.

(31) Galitski, V.; Karnakov, B.; Kogan, V.; Galitski, V., Jr. *Exploring Quantum Mechanics: A Collection of 700+ Solved Problems for Students, Lecturers, and Researchers*; Oxford University Press: Oxford, UK, 2013.

(32) Galitskii, V. M.; Kamakov, B. M.; Kogan, V. I. *Zuduchi po kvantovoi mekhanike (Problems in Quantum Mechanics)*; Nauka: Moscow, 1984.

(33) Watson, G. N., *Treatise on the Theory of Bessel Functions*, 2nd ed.; Cambridge University Press: New York, 1966.

(34) Korn, G. A.; Korn, T. M. *Mathematical Handbook for Scientists and Engineers*; McGraw-Hill: New York, 1961.

(35) Eisler, S.; Slepkov, A. D.; Elliott, E.; Luu, T.; McDonald, R.; Hegmann, F.; Tykwinski, R. Polyynes as a Model for Carbyne: Synthesis, Physical Properties, and Nonlinear Optical Response. *J. Am. Chem. Soc.* **2005**, *127*, 2666−2676.

(36) Chalifoux, W.; Tykwinski, R. Synthesis of Polyynes to Model the sp-Carbon Allotrope Carbyne. *Nat. Chem.* **2010**, *2*, 967−971.

(37) Berkovitch-Yellin, Z.; Leiserowitz, L. Electron Density Distribution in Cumulenes: an X-Ray Study of Tetraphenylbutatriene at 20 and −160 °C. *Acta Crystallogr.* **1977**, *33*, 3657−3669.